The First- and Second-Order Fermi Acceleration Processes in BL Lacertae Objects

Bidzina Kapanadze [1,2]

1   E. KharadzeAbastumani Astrophysical Observatory, Ilia State University, Colokashvili Av. 3/5,
    0162 Tbilisi, Georgia; bidzina_kapanadze@iliauni.edu.ge; Tel.: +995-577414299
2   INAF, OsservatorioAstronomico di Brera, Via E. Bianchi 46, I-23807 Merate, Italy

check for
updates

Abstract: BL Lacertae objects constitute a rare class of active galactic nuclei with extreme observational features attributed to the Doppler-boosted emission from a relativistic jet, closely aligned to our line-of-sight. Their spectral energy distribution, extending over 17–19 orders of frequency from radio to the TeV energy range, is of non-thermal origin and shows a typical two-component structure. The lower-energy component, ranging from the radio to X-rays in the high-energy peaked BL Lacertae sources, is widely accepted to be a synchrotron radiation emitted by ultra-relativistic charged particles, to be initially accelerated via the Blandford–Znajek mechanism or magneto-hydrodynamic processes in the vicinity of the central super-massive black hole. However, the accelerated particles should lose the energy, sufficient for the emission of the keV-GeV photons, very quickly and the source can maintain its flaring state on the daily-weekly timescales only if some additional acceleration mechanisms are continuously at work. According to different studies and simulations, the particles can gain tremendous energies due to the propagation of relativistic shocks through the jet: By means of first-order Fermi mechanism at the shock front, or they undergo an efficient stochastic (second-order Fermi) acceleration close to the shock front, in the turbulent jet medium. Our intensive X-ray spectral study of TeV-detected, bright BL Lacertae objects (Mrk 421, 1ES 1959+650, Mrk 501) often show the signatures of the stochastic acceleration, while those related to the first-order Fermi process arefound relatively rarely. The TeV-undetected sources (1H 1516+660, BZB J1341+3959, BZB J1237+6258) mostly do not show the signatures of the efficient stochastic acceleration in their jets.

Keywords: BL Lacertae objects: general; galaxies: active

1. Introduction

The BL Lacertae objects constitute an extreme class of active galactic nuclei (AGNs) featuring non-thermal continuum emission stretching from radio to TeV-band (17–19 orders of frequency), absence of emission lines, strong flux variability in all spectral bands, compact and flat-spectrum radio emission, apparent superluminal motion of some components, high and variable radio/optical polarization, strong X-ray and γ-ray emissions [1]. These properties are explained by the presence of a super-massive black hole (SMBH; with masses $M\sim10^8$–$10^9\ M_\odot$) in the center of the elliptical host galaxy, along with the inherent accretion disc (AD) and relativistic jet closely aligned to the observer (see Reference [2], and references therein).

One of the open problems consists in the nature of the physical mechanism of launching relativistic jets and acceleration of charged particles, responsible for the non-thermal spectral energy distribution (SED), to the tremendous energies. The SED of BL Lacertae objects is characterized by two broad peaks in the log ν–log νF_ν representation. The lower-frequency SED component is explained via synchrotron radiation emitted by relativistic electrons in the jet, while there is a variety of models for the origin of the higher-energy bump, with the three most frequently considered scenarios: An inverse Compton (IC)

scattering of synchrotron photons by the their "parent" electrons (so-called synchrotron self-Compton model, SSC; Reference [3]); ambient photons scattered by the jet ultra-relativistic electrons (external Compton, EC; Reference [4]), hadronic processes (Reference [5], and references therein).

One of the open problems, related to the nature of BL Lac objects, consists in the very powerful processes which are responsible for the jet launching and for the acceleration of the particles to the tremendous energies within it (necessary for the generation of X-ray and γ-ray photons via the synchrotron and IC mechanisms). The current paradigm of the launching and acceleration of the relativistic jets attributes a key role to the magnetic fields, allowing extraction of the energy stored in a rapidly spinning SMBH via the Blandford–Znajek (B-Z) mechanism [6]. Consequently, the originally almost pure electromagnetic jet power is spent to accelerate the channeled matter, until an equi-partition between the magnetic and kinetic energy fluxes is established [7]. However, the electrons, accelerated to ultra-relativistic energies by the B-Z mechanism, lose their energy via the emission of X-ray photons (plus the IC-scattering), very quickly: The radiative lifetimes are of the order of one hour, corresponding to minutes in the observer's frame (assuming the Doppler factor δ~10; Reference [8]).

The flaring keV-GeV states, observed in BL Lac objects on daily-weekly timescales and X-ray emission detected at the sub-parsec, parsec, kilo-parsec and sometimes even at the Mega-parsec distances (Chandra observations; see, e.g., Reference [9]) demonstrates that some local acceleration mechanisms should be continuously at work in BL Lac jets.

Moreover, rapid TeV variability observed in BL Lac objects (e.g., in PKS 2155-304 and Mrk 501; see References [10,11], respectively) is characterized by timescales of a few minutes which are shorter, by at least an order of magnitude, than the light-crossing time of the central SMBH with a typical mass. Therefore, the ultra-fast TeV variability should be associated to the small jet regions rather than the central region. With the observed variability timescale t_{var} and jet Lorentz factor Γ, the flare should occur at a distance greater than $ct_{var}\Gamma^2$ [12], yielding that the flaring region is situated at a distance in excess of 100 Schwarzschild radii from the central engine, i.e., beyond the distance of the maximum acceleration of the particles via the B-Z mechanism [6]. These results show that the particles are accelerated close to the emission region.

The most plausible "additional" acceleration mechanisms for the particles responsible for the generation of the non-thermal emission in BL Lac objects are as follows: (1) Diffusive shock acceleration (DSA, or the first-order Fermi mechanism [13]), which operates at the front of relativistic shocks propagating down the jet; (2) stochastic (second-order Fermi) acceleration by the magnetic turbulence in the shocked jet area [14].

The viability of the first and second-order Fermi mechanisms is confirmed by the presence of X-ray spectral curvature in high-energy-peaked BL Lac objects (HBLs, with the synchrotron SED peak situated at the UV–X-ray frequencies; Reference [15]), i.e., their X-ray spectra are fitted with the log-parabolic (LP) model (see Reference [8] and Figure 1 for the corresponding example):

$$F(E) = K(E/E_1)^{-(a+b\log(E/E_1))} \, \mathrm{ph/cm^2/s}, \tag{1}$$

where E is the photon energy; E_1: *the* reference energy, generally fixed to 1 keV; a: the photon index at E_1; b: the curvature parameter. Such spectra can be produced by the relativistic electron population with the log-parabolic energy distribution, yielding the LP photon spectra more naturally than the original interpretation of the spectral curvature in terms of radiation cooling of the high energy electron population, injected with a power-law spectrum [8]. On the other hand, the generation of the LP energy distribution of electrons is expected in the framework of the first and second-order Fermi acceleration with the inherent observables, discussed in this paper.
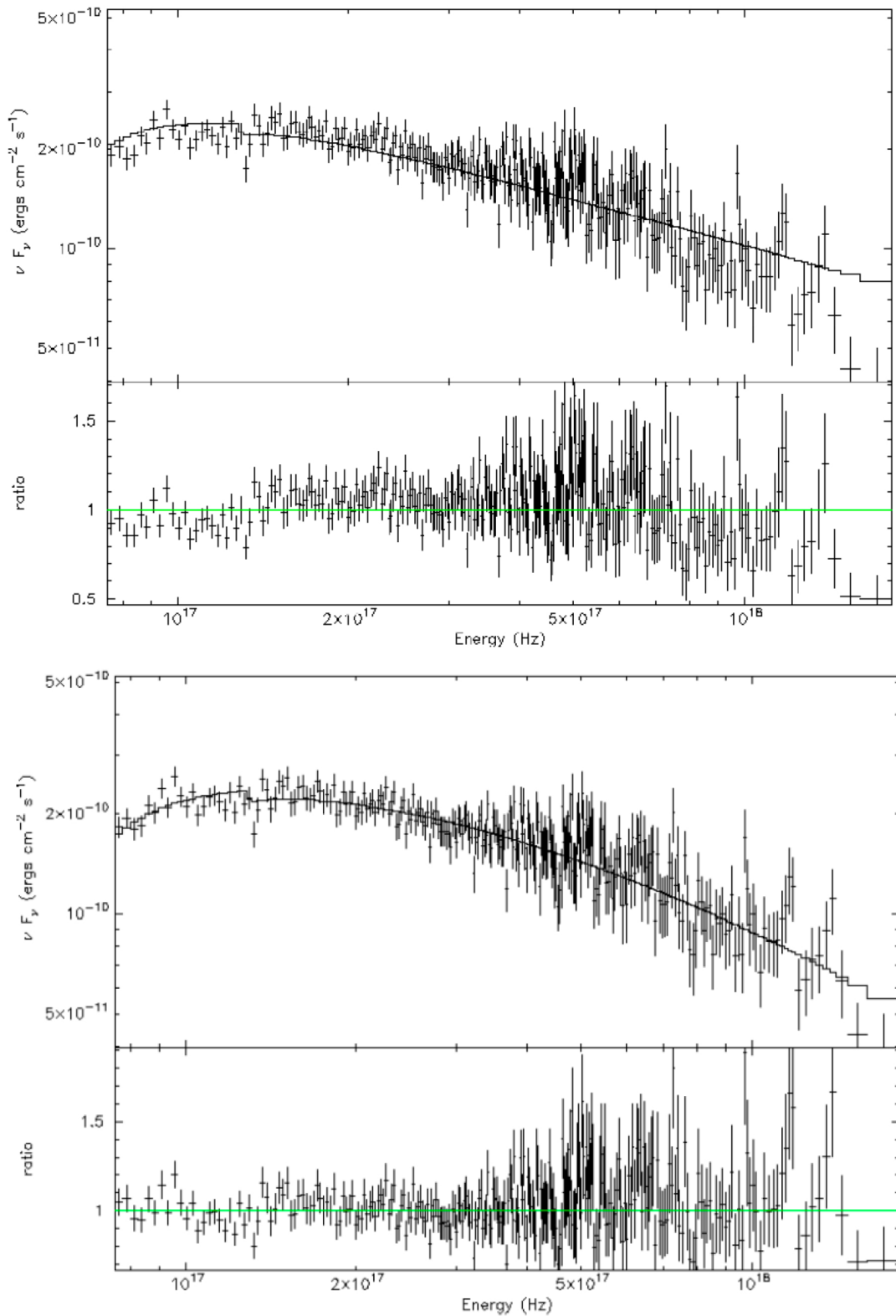
Figure 1. Upper panel: A simple power-law (left) fit to the 0.3–10 keV spectrum of Mrk 421 extracted from the observation ObsID 00030352115 (24 March 2009) made by X-ray Telescope onboard the satellite Swift, yielding the reduced Chi-squared (χ_r^2) value of 1.40 with 270 degrees-of-freedom (d.o.f.) and a prominent trend in the residuals. In the **lower panel**, the same spectrum is fitted with the log-parabolic model, yielding $\chi_r^2 = 1.09$ with 269 d.o.f., and the distribution of the fit residuals show that the model is acceptable for this spectrum. It shows a significant curvature with $b = 0.30 \pm 0.03$.

2. The Origin of X-ray Spectral Curvature

The first-order Fermi acceleration relies on the repeated scatter of charged particles by the magnetic fluctuations: They gain energy whenever two subsequent scattering centers are moving towards each other, leading to the "head-on" collision. The suitable conditions are provided around the shock wave, where a relativistic particle, crossing the shock front, always "sees" the scattering centers on the other side of the shock approaching [16].

During this process, a particle gains energy by multiple crossing the shock front and its energy can be increased by a factor of Γ^2 for the first cycle, and by a factor of ~2 thereafter [16]. The duration of each cycle, as well as the probability for a particle to be injected into the acceleration zone, or re-cross the shock front, depends on the details of the scattering of the particles in the turbulent plasma and the geometry of the shock. Eventually, a particle escapes from the "acceleration zone" and undergoes a cooling by the synchrotron radiation and IC-scattering in the magnetic field behind it (so-called "emission zone"; Reference [13]).

Generally, first-order Fermi mechanism yields a power-law spectrum [8]:

$$N(> \gamma) = N_0(\gamma/\gamma_0)^{-s+1}, \tag{2}$$

where $N(> \gamma)$ is the number of the particles having the Lorentz factor higher than γ; s—the spectral index given by

$$s = -(\log p)/(\log \varepsilon) + 1, \tag{3}$$

with the probability p that a particle undergoes an acceleration step i, characterized by the energy gain ε. A log-parabolic energy spectrum is expected when the parameter p is dependent on the energy:

$$p_i = g/\gamma_i^l, \tag{4}$$

where p_i and γ_i are the probability and the particle's energy at the acceleration step i; g and l are the positive constants. Consequently, the probability of the particle's subsequent acceleration is lower when its energy increases. This situation may occur when particles are confined by a magnetic field with a confinement efficiency decreasing for an increasing gyration radius [8]. This is so-called energy-dependent acceleration scenario (EDAP), explains the origin of the log-parabolic particle and photon spectra.

An LP particle energy distribution can be also established via the stochastic (second-order Fermi) mechanism operating in the turbulent jet area. It accelerates particles using the scattering centers moving towards each other even without differences in the actual flow speed (see References [14,16]). Note that the relativistic shocks in the jets of BL Lacertae objects can strongly amplify a turbulence (References [17,18]). The Alfven waves in the turbulent structures, situated downstream to the relativistic shock, can provide promising conditions for the efficient stochastic acceleration [19]. The stochastic mechanism is not tied to the plasma speed, and, therefore, it can continue to accelerate particles far away from the shock front and during the significantly longer time interval than the first-order Fermi process (when sufficient turbulence is present; Reference [16]).

According to References [20,21], the log-parabolic energy distribution represents a general solution of the energy- and time-dependent Fokker–Planck equation that includes the systematic (e.g., B-Z mechanism) and stochastic (momentum diffusion due to resonant interactions with turbulent magneto-hydrodynamic modes) accelerations, along with the radiative and adiabatic cooling, particle escape and injection terms.

3. Results

3.1. First-Order Fermi Acceleration

According to Reference [8], the EDAP scenario predicts a positive correlation between the parameters *a* and *b*. These authors found a strong positive *a*-*b* correlation (with the correlation coefficient

$p = 0.94$) from the 0.1–10 keV observations of the nearby, bright HBL source Mrk 421 (redshift $z = 0.031$) performed with the satellite *BeppoSAX*.

We have performed an intensive search of the aforementioned correlation for the bright HBLs in the 0.3–10 keV energy range, based on the rich archival material, obtained with X-ray Telescope (XRT; Reference [22]) onboard Neil Gehrels Swift Observatory [23]. The unscreened event files were reduced, calibrated and cleaned according to the standard procedures, using the latest versions of the HEASOFT package and the Swift calibration database. We extracted the 0.3–10 keV spectra with XSELECT. The ancillary response files (ARFs) were generated using the XRTMKARF task, with the corrections applied to account for the different instrumental defects. The latest response matrix from the XRT calibration files has been used. The instrumental channels were combined to include at least 20 photons per bin using the GRPPHA task. Using the XSPEC package, we performed the X-ray spectral analysis by fixing the N_H absorbing column density to the Galactic value for the particular source and fitting the 0.3–10 keV spectrum with three different models, generally applicable for the spectra of BL Lacertae objects: (1) The log-parabolic (LP) model (see Equation (1)). Determining the values of the parameters from the spectral fit, the position of the syncrotron SED peak is given by [8]

$$E_p = E_1 10^{(2-a)/2b} \text{ keV};\tag{5}$$

(2) simple power-law $F(E) = KE^{-\Gamma}$, with Γ: the photon index throughout the observation band; (3) broken power-law (see https://heasarc.gsfc.nasa.gov/xanadu/xspec/manual/XSmodelBknpower.html for details). For each spectrum, the model validity was checked using the reduced chi-squared (or the task GOODNESS when the Cash statistics was applied in the case of the poor spectra), the distribution of the fit residuals, and the *F*-test. The original results are provided in References [24–33], showing that the 0.3–10 keV spectra of HBLs generally are well-fit with the LP-model.

In contrast to Reference [8], we have revealed significantly weaker correlations with $p = 0.21(0.07) - 0.56(0.12)$ between the curvature parameter and photon index for Mrk 421 from the Swift-XRT observations performed in 2005–2008, 2009–2012, and February 2015 (see Figure 2a–c and References [24,25,27]).
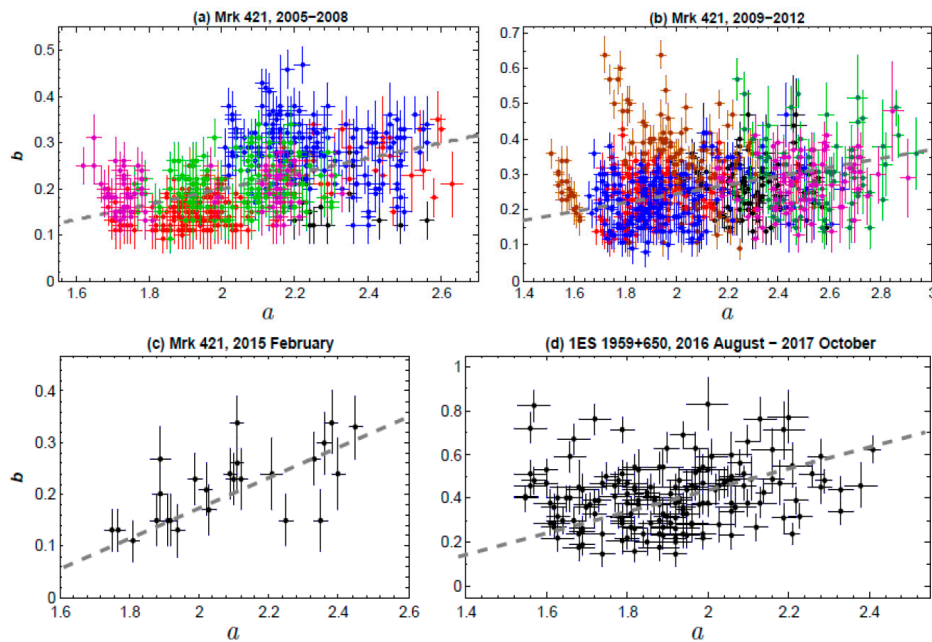
Figure 2. The *a-b* correlation for Mrk 421 (**a–c**) and 1ES 1959+650 (**d**) observed with Swift-XRT in different periods (reproduced from References [24,25,27,28]). In (**a,b**), the colored points correspond to the different intervals of the periods 2005–2008 and 2009–2012 (see References [24,25] for details). Gray dashed lines represent linear fits to scatter plots.

Note that the source did not show a statistically significant correlation during January 2013 to January 2015 (including the giant X-ray outburst in 2013 April; see Reference [26]) and in March to June 2015 [28]. A similar situation was during some time intervals of the 2005–2012 period (see Figure 2a,b and References [24,25]). Moreover, no positive *a-b* correlation was found from the Swift-XRT observations of 1ES1959+650 during April 2005 to July 2016 (see References [29–31]), Mrk 501 in March to October 2014 [32], PKS 2155-304 during 2005 to 2013 [33].

Note that EDAP involves a rapid injection of very energetic particles into the emission zone rather than the gradual acceleration [34]. For example, in the Bohm limit, for an electron with $\gamma \sim 10^4$, magnetic field strength of 1 Gauss and relativistic shock (with the velocity $v_s \to c$), the acceleration timescale is as short as a few milliseconds and can be considered as instantaneous [16]. Consequently, the source expected to show a clockwise (CW) spectral evolution in the hardness ratio (HR)-flux plane (see Reference [34]; in our study, the hardness ratio is defined a ratio of the de-absorbed 2–10 keV to 0.3–2 keV fluxes). The corresponding example is presented in Figure 3, where the HR-flux plane is constructed for the Swift-XRT observations of Mrk 421 performed during February 2015, i.e., in the epoch of the positive *a-b* correlation presented in Figure 2c.
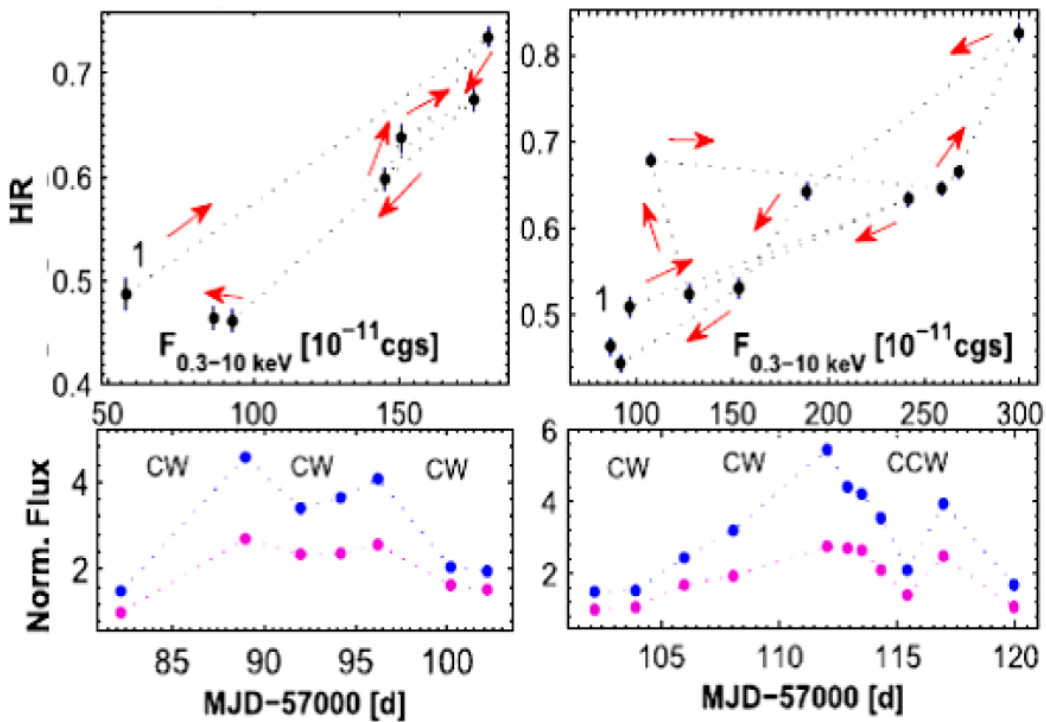

Figure 3. The hardness ratio (HR)-flux planes for the Swift-XRT observations of Mrk 421 in February 2015, along with the normalized soft 0.3–2 keV (magenta points) and hard 2–10 keV (blue points) fluxes plotted as a function of time (reproduced from Reference [27]). The light curves for hard fluxes are shifted arbitrarily for a better resolution. In each panel, the start point is denoted by "1". The acronym "cgs" stands for erg cm^{-2} s^{-1}.

For protons, however, the mass and acceleration timescale are 1000 times larger than that for electrons. Consequently, no instantaneous injection is expected for the emission zone with significant hadron contribution. A similar situation is for the electron-positron jet with the magnetic field strength significantly lower than 1 Gauss [16]. The corresponding cases (counter-clockwise spectral evolutions in the epochs of positive *a-b* correlation) also have been revealed in the framework of our study (see, e.g., References [24,25,28]).

3.2. Stochastic Acceleration

According to Reference [35], the electrons in the jets of TeV detected BL Lacertae objects (TBLs, including X-ray bright HBLs) should undergo a more efficient stochastic acceleration, resulting in broad synchrotron SEDs with $b\sim0.3$ compared to the TeV-undetected ones (UBLs) showing $b\sim0.7$. This suggestion is fully confirmed by the Swift-XRT observations of Mrk 421 during 2005–2015: more than 90% of the b values are ~0.3 or smaller (see References [24–27] and Figure 4a–d).
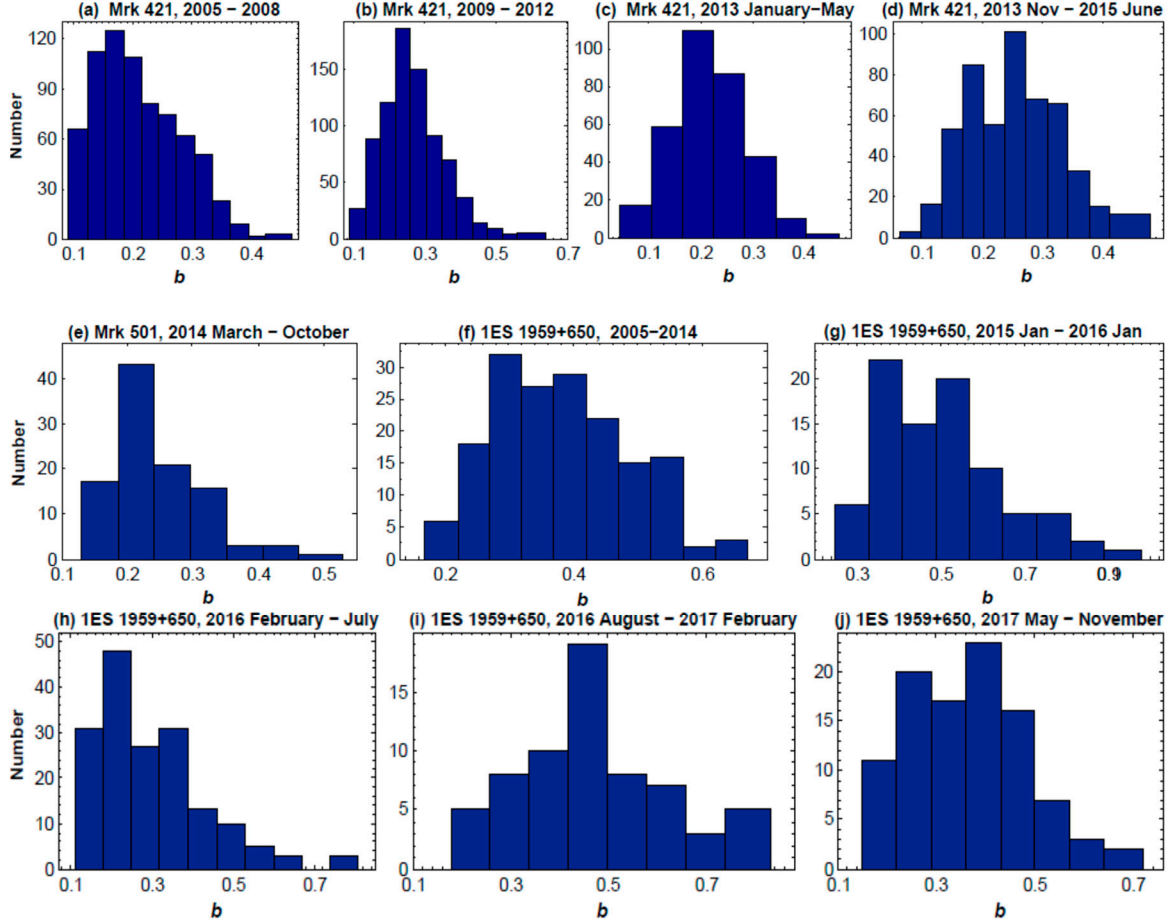
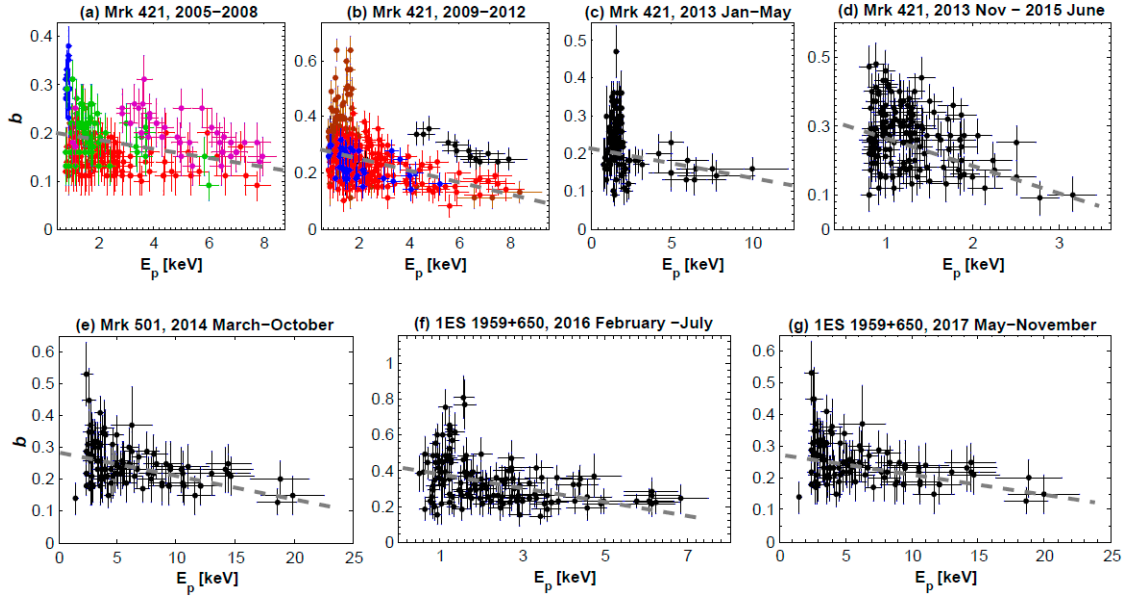**Figure 4.** The distribution of the values of the curvature parameter correlation for Mrk 421 (**a**–**d**), Mrk 501 (**e**) and 1ES 1959+650 (**f**–**j**) observed with Swift-XRT in different periods (reproduced from References [24–32]).

Note that the E_p-b anti-correlation is also expected in the case of the efficient stochastic acceleration (see, e.g., Reference [21]). In fact, this anti-correlation was detected for each of the cases presented in Figure 4a–d, although it was weak or very weak (Figure 5a–d).

A similar situation is revealed in the case of the Swift-XRT observations of Mrk 501 performed in March–October 2014 (see Figures 4 and 5). However, another TeV-detected, bright HBL source 1ES 1959+650, sometimes poses a challenge to the suggestion about the efficient stochastic acceleration of the particles in the TBL jets [35]. Namely, mostly relatively large spectral curvature was observed during January 2015 to January 2016: A total of 85% of the spectra showed $b > 0.4$ (a conventional threshold between larger and smaller curvatures), and more than 50% of the spectra were characterized by $b > 0.5$ (Figure 4g). Similarly, the weighted mean value of the curvature parameter $<b> = 0.47\%$ and 63% of the values larger than $b = 0.4$ was observed for the same source in August 2016 to February 2017 (Figure 4i). In contrast, 58% of the spectra of 1ES 1959+650 were characterized with the curvatures below this threshold and $<b> = 0.36$ in May to November 2017. Moreover, a strong X-ray flaring

activity of this HBL source during June to July 2016 yielded 95% of the 0.3–10 keV spectra with $b \sim 0.3$, expected in the case of the efficient stochastic acceleration (Figure 4j,h).

Figure 5. The E_p-b anti-correlation for Mrk 421 (**a–d**), Mrk 501 (**e**) and 1ES 1959+650 (**f–g**) observed with Swift-XRT in different periods (reproduced from References [24–28,32]). In (**a,b**), the colored points correspond to the different intervals of the periods 2005–2008 and 2009–2012 (see References [24,25] for details). Gray dashed lines represent linear fits to the scatter plots.

Note also that the bright HBLs frequently exhibit declining optical-UV brightness in the epoch of X-ray flare (see Figure 6 and References [24–30]). A similar behavior was reported in Reference [36] from the multiwavelength observations of Mrk 421 during January to June 2009 and explained by global long-term change in the efficiency of the acceleration mechanism, leading to the shift of the entire synchrotron bump to higherenergies. Namely, this mechanism yields the spectral index of the electron population to become harder, and, consequently, the emission at the rising segment of the synchrotron SED (radio-UV) decrease, while that on the decreasing segment (X-rays) is increasing.
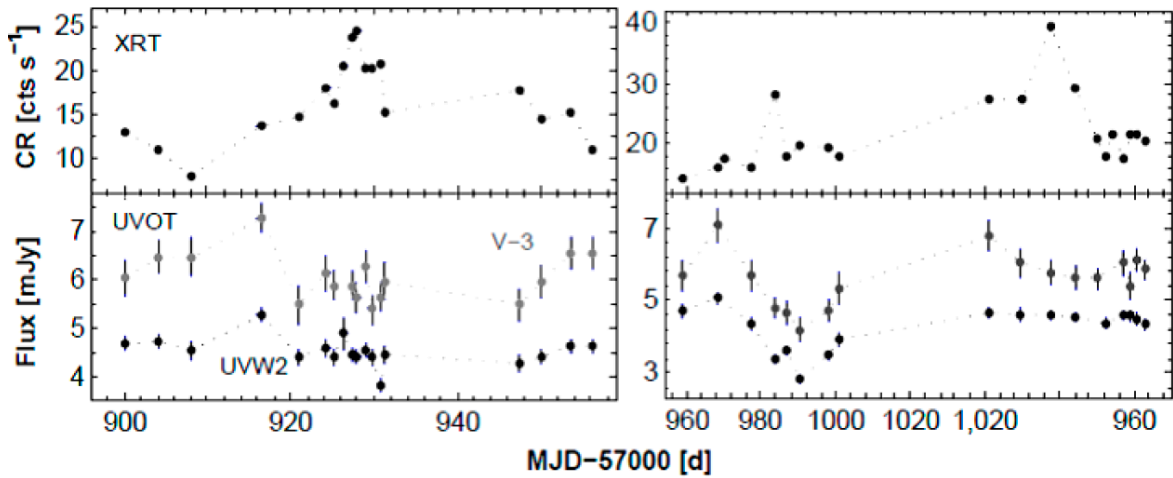

Figure 6. The multiwavelength observations of 1ES 1959+650 performed with Swift-XRT and Ultraviolet-Optical Telescope onboard Swift (Swift-UVOT; reproduced from Reference [28]).

Note that this suggestion is corroborated by our finding of a positive E_p–$F_{0.3\text{–}10\text{ keV}}$ correlation in the epoch of the anti-correlations between the X-ray and optical-UVOT fluxes, i.e., HBLs showed a shift of

the synchrotron SED peak towards higher energies with increasing X-ray flux [see References [24–30]). The simulations performed within Reference [37] demonstrated that the hardening in the electron energy distribution is expected during the stochastic acceleration when these particles have a narrow initial energy distribution with the average energy, significantly higher than the equilibriumenergy.

The simulations also show that the stochastic acceleration is very slow for the jets with low magnetic fields and high matter densities (see, e.g., Reference [16]). In that case, a gradual acceleration of the particles is expected [19], yielding a counter-clockwise (CCW) spectral evolution of the source in the hardness ratio–flux plane (see Reference [34] and Figure 7 for the corresponding example).
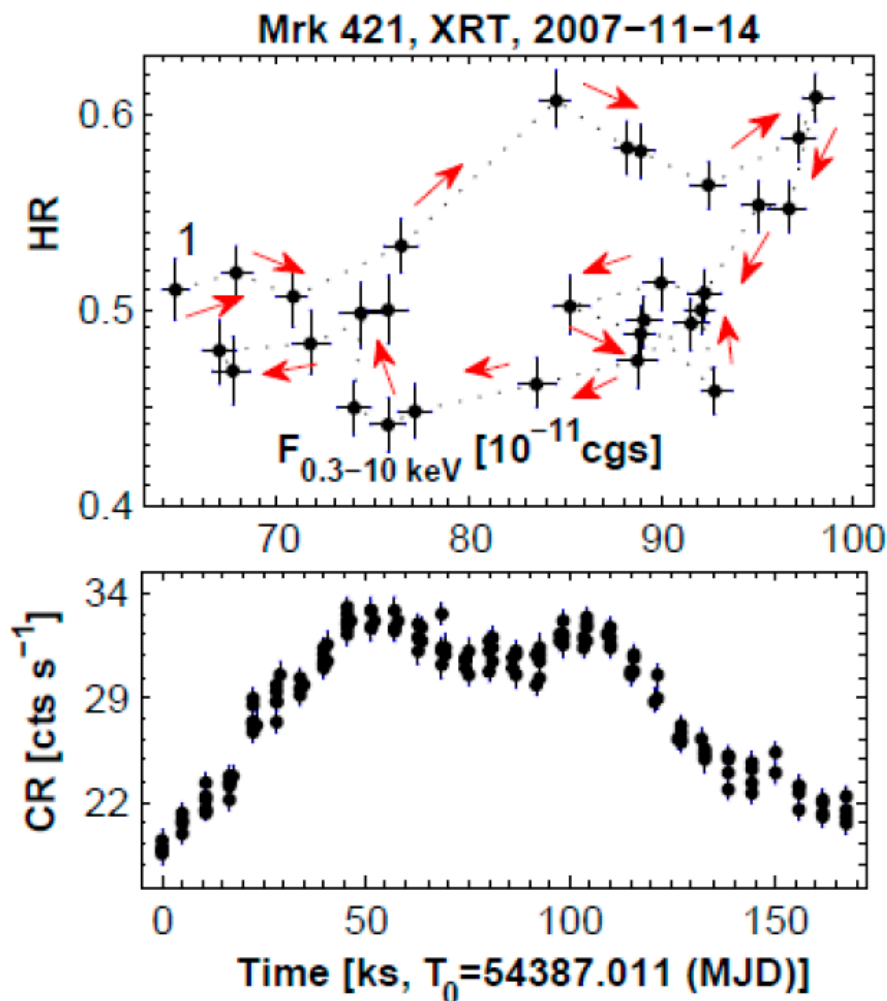
Figure 7. HR-flux plane (**upper panel**) from the densely-sampled, prolonged Swift-XRT observation of the intra-day 0.3–10 keV flare (**lower panel**) in Mrk 421 performed on 14 November 2007. This flare was characterized by the features of efficient stochastic acceleration—low spectral curvature and the E_p-b anti-correlation (reproduced from Reference [24]).

4. Discussion and Conclusions

HBLs represent one of the most extreme particle accelerators in the universe: They generally are bright sources in the X-ray energy range where the injection and radiative evolution of freshly accelerated particles can be tracked (especially in the nearby bright sources Mrk 421, Mrk 501, 1ES 1959+650, PKS 2155-304). Note that these sources allow us to detect extreme flux and spectral variability on timescales of a few hundred seconds, especially in the flaring states (see References [24–33]).

The B-Z mechanism, widely accepted to be responsible for the jet launching and acceleration of the particles up to ultra-relativistic energies within the hundred Swarzschild radii, is not sufficient

for explaining the X-ray and γ-ray emissions generated on sub-parsec, parsec, kilo-parsec distances from the central engine, as well as the flaring behavior observed in the keV–TeV energy range. Therefore, some additional, in-situ acceleration processes are necessary to reconcile the modeling and observational results.

The most frequently considered, additional "mechanisms" are the first and second-order Fermi accelerations, related to the propagation of relativistic shocks and turbulent structures in the jets (corroborated by the observed log-parabolic X-ray and γ-ray spectra). The features of both acceleration mechanisms are revealed via our intense X-ray spectral study of nearby bright HBLs. However, those related to the stochastic (second-order Fermi) process are observed more frequently than the observables expected in the case of EDAP (a variety of first-order Fermi mechanism).

Moreover, X-ray observations of bright HBLs show a change in the turbulence spectrum in some epochs. According to the simulations performed by Reference [21], the source may show a relationship between the synchrotron SED peak position E_p and the flux at the peak S_p as follows

$$S_p \propto E_p^\alpha,$$

with the value of the exponent $\alpha = 0.6$: the parameters q(the exponent describing the turbulence energy distribution $W(k)$ in terms of the wave number k with a power-law $W(k) \sim k^{-q}$) is variable during the second-order Fermi acceleration process. Namely, there is a transition from the Kraichnan-type ($q = 3/2$) into the "hard-sphere" ($q = 2$) spectrum. Figure 8 provides the Swift-XRTobservations of Mrk 421, Mrk 501 and 1ES 1959+650 in some epochs, which demonstrate the $S_p \propto E_p^\alpha$ relation with the values of the exponent α close to 0.6, i.e., showing the change in the energy spectrum of the turbulence, responsible for the stochastic acceleration in the jets of the aforementioned HBLs. Consequently, our study shows as the importance of the stochastic acceleration in the jets of BL Lacertae objects, as well as the presence of the variable turbulent conditions in these extreme AGN areas. On the other hand, the aforementioned change hints at the presence of the cooling-dominated X-ray flares with the electron energy distribution approaching to equilibrium as predicted by the simulations performed within Reference [21].

We suggest the possibility of a complex acceleration process of the electrons to the energies necessary for the emission of X-ray photons via the synchrotron mechanism: A joint operation of (i) "classical" first-order Fermi acceleration yielding a power-law energy spectrum, (ii) EDAP, (iii) stochastic acceleration etc. For example, the simulations performed within Reference [37] showed that the charged particle can be accelerated at the shock front by the first-order Fermi process and then continue gaining an additional energy by means of the stochastic mechanism in the shock downstream region. Eventually, the particle will be able to re-enter the shock acceleration region and repeat the combined acceleration cycle. Consequently, a positive *a-b* correlation will weaken and may not even be observed. Consequently, the features related to the first or second-order Fermi acceleration, e.g., the E_p–*b* and *a-b* correlations, can be weakly expressed and even absent.

The EDAP scenario generally predicts a rapid injection of very energetic particles into the emission zone and a CCW-type evolution of the source in the HR-flux plane during the X-ray flare is expected. However, the acceleration may not be "instantaneous" under some astrophysical conditions (e.g., weak magnetic field, absence of the Bohm limit during the scattering of the electrons off the magnetic irregularities, significant hadronic contribution), and the source will trace an opposite spectral loop. In the case of the second-order Femi process, operating in the purely hadron-less pair (electron-positron) plasma, the acceleration timescale can be short and even instantaneous if the shocked jet medium is characterized by low matter density and sufficiently high magnetic field [16]. Under such circumstances, a BL Lacertae source may show a CW-type loop in the epoch of efficient stochastic acceleration.
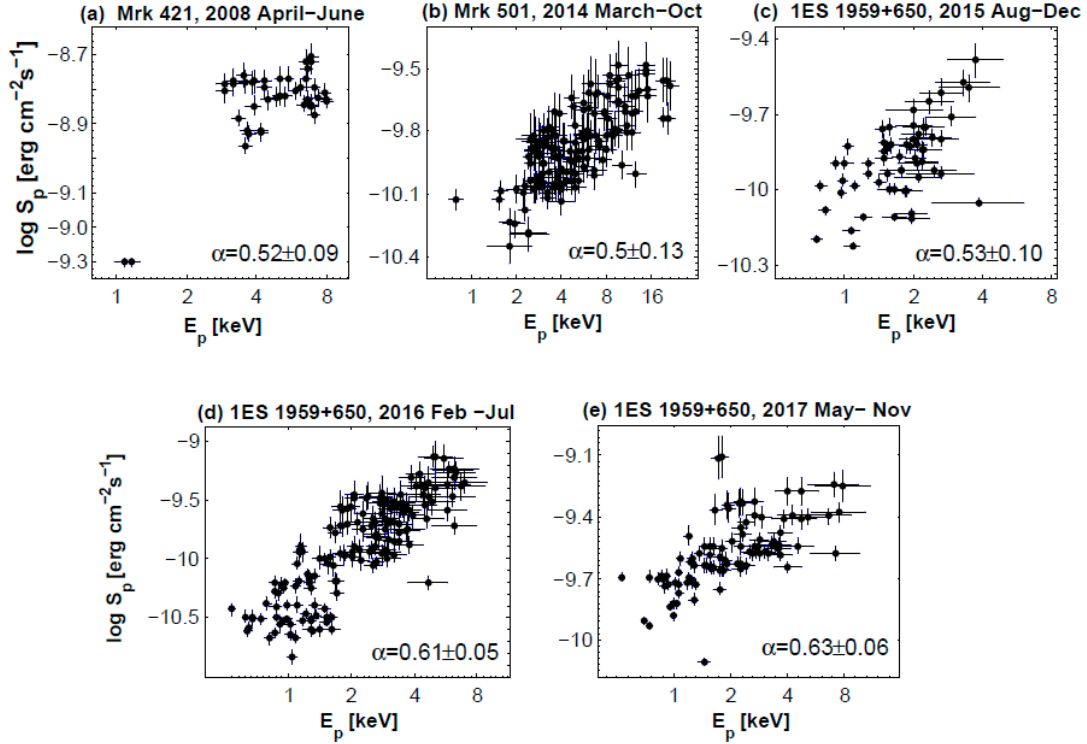
Figure 8. The $S_p \propto E_p^\alpha$ relationship for the bright HBLs in different periods with $\alpha \sim 0.6$ (reproduced from References [24,28,31,32]).

In fact, HBLs rarely show the epochs or particular X-ray flares characterized by purely CW or CCW loops. For example, we often observe a change from the CWW-type spectral evolution into the opposite one and vice versa. The corresponding example is provided in Figure 9, presenting the HR-flux planes from the epoch of efficient stochastic acceleration in the jet of 1ES 1959+650 (featured by low spectral curvature and by the E_p–b anti-correlation; see Figures 4 and 5). We attribute such changes to the subsequent shock passage in the jet areas with different physical conditions: The first-and second-order Fermi accelerations in the areas with different matter density, composition and magnetic field may yield as instantaneous, as well as a gradual acceleration of the electrons (resulted in both CW and CCW loops in the HR-flux plane).
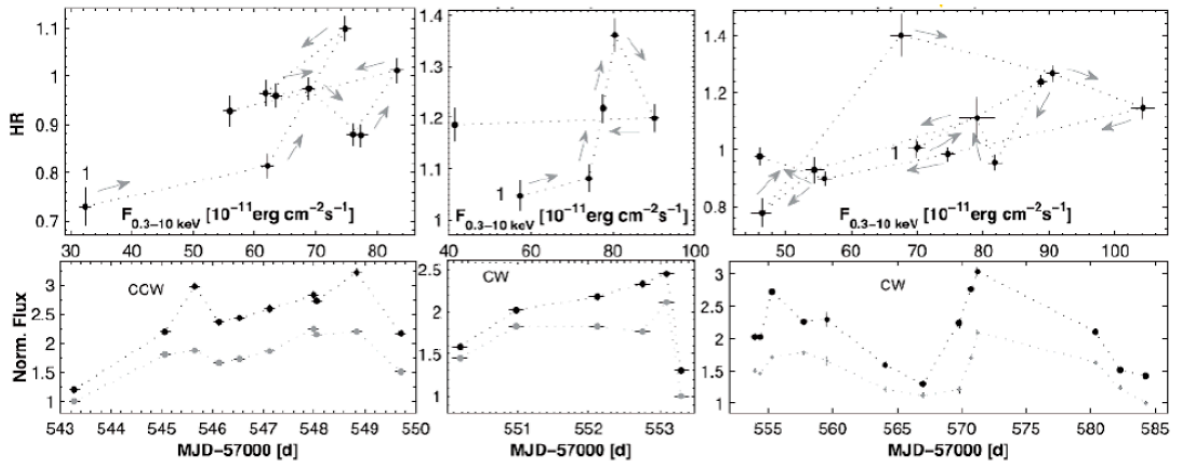
Figure 9. HR-flux planes for the epoch of strong X-ray flaring activity of 1ES 1959+650 in May–November 2017, along with normalized soft 0.3–2 keV (black points) and hard 2–10 keV (gray points) fluxes plotted as a function of time (reproduced from Reference [28]).

Note that Mrk 421 showed an unprecedentedly high percentage of the power-law spectra (28%) in 2005–2008 that is not common for the HBL sources (see Reference [24]). As we have noted above, this period showed the importance of the EDAP process, although the parameter *l* probably was not dependent on the particle's energy in some cases (required for the efficient EDAP). Therefore, a power-law energy distribution of X-ray emitting electrons was established. On the other hand, this distribution can be related to fact that the turbulent magnetic field was not sufficiently strong for the efficient second-order Fermi acceleration. Consequently, the properties of the magnetic field in the jet of Mrk 421 were variable in 2005–2008, and sometimes it was not characterized by the confinement efficiency decreasing with a rising particle's energy. Our results also show that the magnetic field properties sometimes were rapidly variable within the jet emission zone (see References [24–27]): Bright HBLs showed a transition from a log-parabolic spectrum into a power-law one, and vice versa, within 1-ks Swift-XRT exposures.

Finally, TBLs often show an Optical-UV decline along with the X-ray flares, hinting at the stochastic acceleration of the electrons characterized by narrow initial energy distribution (as predicted by the simulations).

Conflicts of Interest: The author declares no conflict of interest.

References

1. Falomo, R.; Pian, E.; Treves, A. An optical view of BL Lacertae objects. *Astron. Astrophys. Rev.* **2014**, *22*, 37. [CrossRef]
2. Blandford, R.D.; Rees, M.J. *Pittsburgh Conference on BL Lac Objects*; Wolfe, A.M., Ed.; University Pittsburgh: Pittsburgh, PA, USA, 1978; p. 328.
3. Marscher, A.P.; Gear, W.K. Models for high-frequency radio outbursts in extragalactic sources, with application to the early 1983 millimeter-to-infrared flare of 3C 273. *Astrophys. J.* **1985**, *298*, 114. [CrossRef]
4. Dermer, C.D.; Schlickeiser, R.; Mastichiadis, A. High-energy gamma radiation from extragalactic radio sources. *Astron. Astrophys.* **1992**, *256*, L27–L30.
5. Mannheim, K.; Biermann, P.L. Gamma-ray flaring of 3C 279—A proton-initiated cascade in the jet? *Astron. Astrophys.* **1992**, *253*, L21–L24.
6. Tavecchio, F.; Ghisellini, G. On the magnetization of BL Lac jets. *Mon. Not. R. Astron. Soc.* **2016**, *456*, 2374–2382. [CrossRef]
7. Tchekhovskoy, A.; McKinney, J.C.; Narayan, R. Efficiency of Magnetic to Kinetic Energy Conversion in a Monopole Magnetosphere. *Astrophys. J.* **2009**, *699*, 1789–1808. [CrossRef]
8. Massaro, E.; Perri, M.; Giommi, P.; Nesci, R. Log-parabolic spectra and particle acceleration in the BL Lac object Mkn 421: Spectral analysis of the complete BeppoSAX wide band X-ray data set. *Astron. Astrophys.* **2004**, *413*, 489–503. [CrossRef]
9. Marscher, A.P.; Jorstad, S.G. The Megaparsec-scale X-ray Jet of The BL Lac Object OJ287. *Astrophys. J.* **2011**, *729*, 26. [CrossRef]
10. Aharonian, F.; Akhperjanian, A.G.; Bazer-Bachi, A.R.; Behera, B.; Beilicke, M.; Benbow, W.; Berge, D.; Bernlöhr, K.; et al. An Exceptional Very High Energy Gamma-Ray Flare of PKS 2155-304. *Astrophys. J.* **2007**, *664*, L71–L74. [CrossRef]
11. Albert, J.; Aliu, E.; Anderhub, H.; Antoranz, P.; Armada, A.; Baixeras, C.; Barrio, J.A.; Bartko, H.; Bastieri, D.; Becker, J.K.; et al. Variable Very High Energy γ-Ray Emission from Markarian 501. *Astrophys. J.* **2007**, *669*, 862–883. [CrossRef]
12. Begelman, M.C.; Fabian, A.C.; Rees, M.J. Implications of very rapid TeV variability in blazars. *Mon. Not. R. Astron. Soc.* **2008**, *384*, L19–L23. [CrossRef]

13. Kirk, J.G.; Rieger, F.M.; Mastichiadis, A. Particle acceleration and synchrotron emission in blazar jets. *Astron. Astrophys.* **1998**, *333*, 452–458.

14. Tramacere, A.; Giommi, P.; Perri, M.; Verrecchia, F.; Tosti, G. Swift observations of the very intense flaring activity of Mrk 421 during 2006. I. Phenomenological picture of electron acceleration and predictions for MeV/GeV emission. *Astron. Astrophys.* **2009**, *501*, 879–898. [CrossRef]

15. Padovani, P.; Giommi, P. The connection between X-ray-and radio-selected BL Lacertae objects. *Astrophys. J.* **1995**, *444*, 567. [CrossRef]

16. Tammi, J.; Duffy, P. Particle-acceleration time-scales in TeV blazar flares. *Mon. Not. R. Astron. Soc.* **2009**, *393*, 1063–1069. [CrossRef]

17. Marscher, A.P. Turbulent, Extreme Multi-zone Model for Simulating Flux and Polarization Variability in Blazars. *Astrophys. J.* **2014**, *80*, 87. [CrossRef]

18. Mizuno, Y.; Pohl, M.; Niemiec, J.; Zhang, B.; Nishikawa, K.I.; Hardee, P.E. Magnetic field amplification and saturation in turbulence behind a relativistic shock. *Mon. Not. R. Astron. Soc.* **2014**, *439*, 3490–3503. [CrossRef]

19. Virtanen, J.J.P.; Vainio, R. Stochastic Acceleration in Relativistic Parallel Shocks. *Astrophys. J.* **2005**, *621*, 313–323. [CrossRef]

20. Paggi, A.; Massaro, F.; Vittorini, V.; Cavaliere, A.; D'Ammando, F.; Vagnetti, F.; Tavani, M. SSC radiation in BL Lacertae sources, the end of the tether. *Astron. Astrophys.* **2009**, *504*, 821–828. [CrossRef]

21. Tramacere, A.; Massaro, E.; Taylor, A.M. Stochastic Acceleration and the Evolution of Spectral Distributions in Synchro-Self-Compton Sources: A Self-consistent Modeling of Blazars' Flares. *Astrophys. J.* **2011**, *739*, 66. [CrossRef]

22. Burrows, D.N.; Hill, J.E.; Nousek, J.A.; Kennea, J.A.; Wells, A.; Osborne, J.P.; Abbey, A.F.; Beardmore, A.P.; Mukerjee, K.; Short, A.D.; et al. The Swift X-ray Telescope. *Space Sci. Rev.* **2005**, *120*, 165–195. [CrossRef]

23. Gehrels, N.; Chincarini, G.; Giommi, P.; Mason, K.O.; Nousek, J.A.; Wells, A.A.; White, N.E.; Barthelmy, S.D.; Burrows, D.N.; Cominsky, L.R.; et al. The Swift Gamma-Ray Burst Mission. *Astrophys. J.* **2004**, *611*, 1005–1020. [CrossRef]

24. Kapanadze, B.; Vercellone, S.; Romano, P.; Hughes, P.; Aller, M.; Aller, H.; Kharshiladze, O.; Kapanadze, S.; Tabagari, L. Swift Observations of Mrk 421 in Selected Epochs. I. The Spectral and Flux Variability in 2005–2008. *Astrophys. J.* **2018**, *854*, 66. [CrossRef]

25. Kapanadze, B.; Vercellone, S.; Romano, P.; Hughes, P.; Aller, M.; Aller, H.; Kharshiladze, O.; Tabagari, L. Swift Observations of Mrk 421 in Selected Epochs. II. An Extreme Spectral and Flux Variability in 2009–2012. *Astrophys. J.* **2018**, *858*, 68. [CrossRef]

26. Kapanadze, B.; Dorner, D.; Vercellone, S.; Romano, P.; Aller, H.; Aller, M.; Hughes, P.; Reynolds, M.; Kapanadze, S.; Tabagari, L. X-ray Flaring Activity of MRK 421 in the First Half of 2013. *Astrophys. J.* **2016**, *831*, 102. [CrossRef]

27. Kapanadze, B.; Dorner, D.; Romano, P.; Vercellone, S.; Kapanadze, S.; Tabagari, L. Mrk 421 after the Giant X-ray Outburst in 2013. *Astrophys. J.* **2017**, *848*, 103. [CrossRef]

28. Kapanadze, B.; Dorner, D.; Vercellone, S.; Romano, P.; Hughes, P.; Aller, M.; Aller, H.; Reynolds, M.; Tabagari, L. Strong X-ray and Multiwavelength Flaring Activity for 1ES 1959+650, 2016 August–2017 November. *Astrophys. J. Suppl.* **2018**, *238*, 13. [CrossRef]

29. Kapanadze, B.; Romano, P.; Vercellone, S.; Kapanadze, S.; Mdzinarishvili, T.; Kharshiladze, G. The long-term Swift observations of the high-energy peaked BL Lacertae source 1ES 1959+650. *Mon. Not. R. Astron. Soc.* **2016**, *457*, 704–722. [CrossRef]

30. Kapanadze, B.; Dorner, D.; Vercellone, S.; Romano, P.; Kapanadze, S.; Mdzinarishvili, T. A recent strong X-ray flaring activity of 1ES 1959+650 with possibly less efficient stochastic acceleration. *Mon. Not. R. Astron. Soc.* **2016**, *461*, L26–L31. [CrossRef]

31. Kapanadze, B.; Dorner, D.; Vercellone, S.; Romano, P.; Hughes, P.; Aller, M.; Aller, H.; Reynolds, M.; Kapanadze, S.; Tabagari, L. The second strong X-ray flare and multifrequency variability of 1ES 1959+650 in 2016 January-August. *Mon. Not. R. Astron. Soc.* **2018**, *473*, 2542–2564. [CrossRef]

32. Kapanadze, B.; Dorner, D.; Romano, P.; Vercellone, S.; Mannheim, K.; Lindfors, E.; Nilsson, K.; Reinthal, R.; Takalo, L.; Kapanadze, S.; et al. The prolonged X-ray flaring activity of Mrk 501 in 2014. *Mon. Not. R. Astron. Soc.* **2017**, *469*, 1655–1672. [CrossRef]

33. Kapanadze, B.; Romano, P.; Vercellone, S.; Kapanadze, S. The X-ray behaviour of the high-energy peaked BL Lacertae source PKS 2155-304 in the 0.3-10 keV band. *Mon. Not. R. Astron. Soc.* **2014**, *444*, 1077–1094. [CrossRef]

34. Cui, W. X-ray Flaring Activity of Markarian 421. *Astrophys. J.* **2004**, *605*, 662–669. [CrossRef]

35. Massaro, F.; Paggi, A.; Cavaliere, A. X-ray and TeV Emissions from High-frequency-peaked BL Lac Objects. *Astrophys. J.* **2011**, *742*, 662–669. [CrossRef]

36. Aleksić, J.; Ansoldi, S.; Antonelli, L.A.; Antoranz, P.; Babic, A.; Bangale, P.; Barres de Almeida, U.; Barrio, J.A.; Becerra González, J.; Bednarek, W.; et al. The 2009 multiwavelength campaign on Mrk 421: Variability and correlation studies. *Astron. Astrophys.* **2015**, *576*, L32. [CrossRef]

37. Katarzyński, K.; Ghisellini, G.; Mastichiadis, A.; Tavecchio, F.; Maraschi, L. Stochastic particle acceleration and synchrotron self-Compton radiation in TeVblazars. *Astron. Astrophys.* **2006**, *453*, 47–56. [CrossRef]